OPTIMIZATION OF AN OPTICALLY IMPLEMENTED ON-BOARD FDMA DEMULTIPLEXER

J. Fargnoli and L. Riddle

Westinghouse Electric Corp.

Baltimore, Maryland

SUMMARY

Performance of a 30 GHz FDMA uplink to a processing satellite is modelled for the case where the on-board demultiplexer is implemented optically. Included in the perforance model are the effects of adjacent channel interference, intersymbol interference, and spurious signals associated with the optical implementation. Demultiplexer parameters are optimized to provide the minimum bit error probability at a given bandwidth efficiency when filtered QPSK modulation is employed.

INTRODUCTION

Satellite communication using frequency division multiple access (FDMA) on the uplinks and time division multiple access (TDMA) on the downlinks has attracted much interest [1,2]. FDMA on the uplink permits the use of ground transmitters that do not require amplifiers having excessively high power. Also, FDMA does not require complicated network timing. TDMA on the downlink takes advantage of recent developments in satellite on-board processing and switching capabilities to provide high data rate downlinks to VSAT-type ground receivers. In addition, the heavily-used C-band and Ku-band frequencies will be supplemented by higher frequency Ka-band transmission (30 GHz uplink / 20 GHz downlink). This permits the use of smaller ground terminal antennas, but at a cost of higher rain attenuation.

On-board processing is needed to efficiently service multiple users while at the same time minimizing earth station complexity. Figure 1 is a simplified overview of a SATCOM system that services FDMA uplink users. The processing satellite first receives the wideband uplink at 30 GHz and downconverts it to a suitable IF. A demultiplexer then separates the composite IF signal into assigned channels. All channels are then demodulated by "bulk" demodulators, with the baseband signals being routed to the downlink processor for retransmission to the receiving earth stations via a high-rate TDMA 20 GHz downlink. This type of processing circumvents many of the difficulties associated with bent-pipe repeaters. First, uplink signal distortion and interference are not retransmitted on the downlink. Second, downlink power can be allocated in accordance with user needs, independent of uplink transmissions. This allows the uplink users to employ different data rates as well as different modulation and coding schemes. In addition, all downlink users will then have a common frequency standard and symbol clock on the satellite, which is useful for network synchronization.

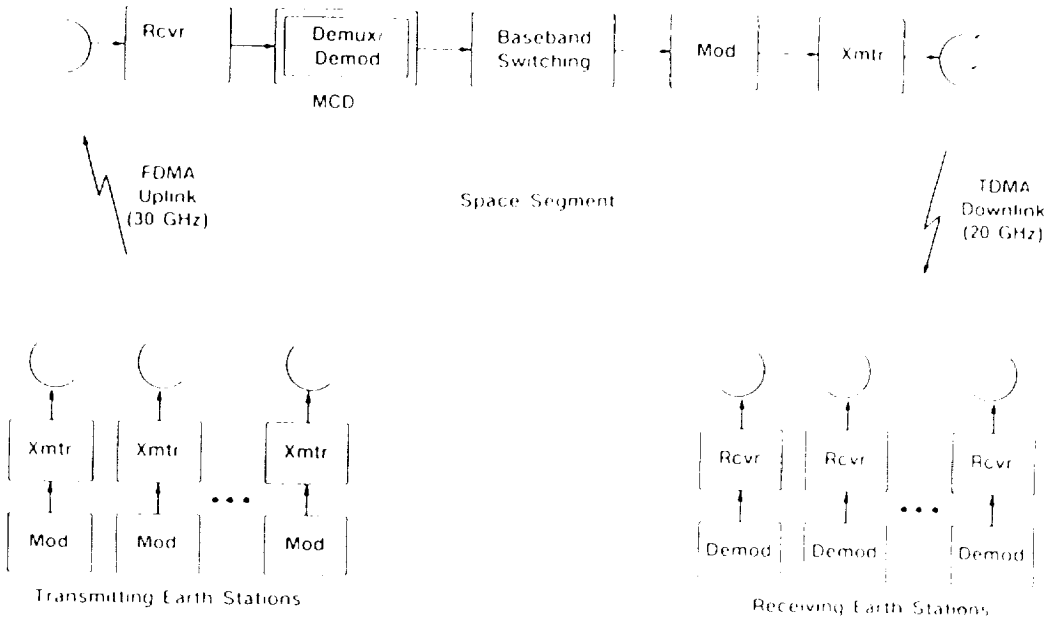

Fig. 1 System overview

These considerations led to a requirement for on-board multichannel demodulators (MCD) that can separate and process the individual transmissions with minimal degradation in bit error probability. Implementation of an MCD is critical because future systems will be highly bandwidth-efficient, which implies very close spacing of the carriers in the composite FDMA uplink.

On-board FDMA demultiplexers can be implemented in a variety of ways. One way is to do a wideband A/D conversion on the uplink signal received at the satellite, followed by digital processing that performs the channel filtering and demodulation operations [3]. However, on-board demultiplexing can also be performed using integrated optics [4,5]. An acousto-optical spectrum analyzer performs both down-conversion and channel filtering, with potential savings in hardware size and weight.

This paper shows how an acousto-optical demultiplexer can be modelled in system performance analyses. Bit error performance is determined in the presence of adjacent channel interference, intersymbol interference, and spurious signals generated by the optical processing.

ON-BOARD DEMULTIPLEXER

An acousto-optical spectrum analyzer (Fig. 2) employing heterodyne detection can function as a channelized receiver. The spectrum analyzer converts the composite FDMA uplink into acoustic waves in a Bragg cell. These acoustic waves modulate a laser beam, and diffract the beam at angles proportional to the uplink RF signal frequencies. Reference beams are also provided to achieve heterodyne operation, resulting in larger dynamic range. The diffracted light impinges on an array of photodetectors, which function as square-law detectors, and the individual photocurrents are routed to QPSK demodulators. Thus, the acousto-optical spectrum analyzer serves as both a channelizer and downconverter, so that

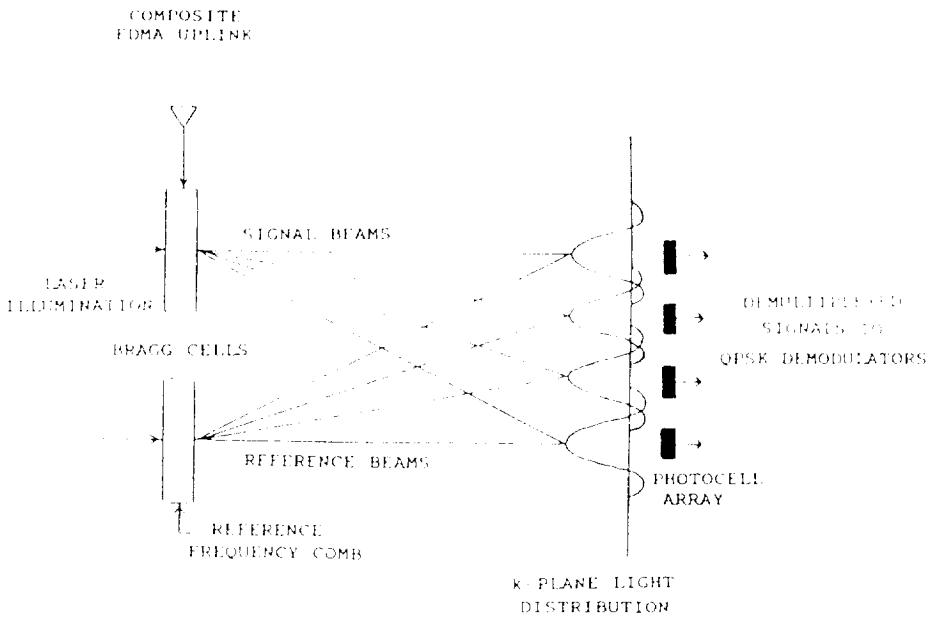

Fig. 2 Acousto-optical Heterodyne Spectrum Analyzer

the composite uplink signal is demultiplexed into separate channels, each at a common IF.

To estimate system performance from a demultiplexer of this type, it is first necessary to determine its transfer function. In a classical linear system, a sinusoidal input to the system results in a sinusoidal output at the same frequency, whose amplitude and phase depend on the frequency. But for the heterodyne system considered here, a sinusoidal input results in not only a sinusoidal output at that frequency, but also sinusoids at $f + \sum nF$, where F is the channel spacing. These spurious sinusoids are generated internal to the demultiplexer by the reference frequency comb. In contrast, the frequencies provided by other transmitters external to the demultiplexer make up the ACI, which is characteristic of all FDMA systems.

DEMULTIPLEXER TRANSFER FUNCTION

As indicated in Fig. 2, two channels constitute the acousto-optical spectrum analyzer: the "signal" channel and the "reference" channel. When the beam has a Gaussian cross section, the light into the signal channel Braqq cell can be expressed as

$$e^{-cSx^2+i2\pi f_L t} \qquad (1)$$

C-3

where f_L is the light frequency, x denotes distance from the center of the Bragg cell, and c_S is a constant determined by the laser beamwidth. This light is modulated by an acoustic wave produced by the input sinusoid of frequency f_S, which can be expressed as

$$e^{i2\pi f_S(t-\frac{x}{v})} \tag{2}$$

where v is the acoustic velocity in the Bragg cell. Therefore, the modulated light out of the cell is the product of (1) and (2), and the signal channel light distribution in the k-plane is the spatial Fourier transform:

$$F_S(k) = e^{i2\pi(f_L+f_S)t}\int_{-\frac{d_S}{2}}^{\frac{d_S}{2}} e^{-c_S x^2 - i2\pi(\frac{f_S}{v}+k)x}dx \tag{3}$$

where d_S is the length of the Bragg cell. Similarly, the light distribution resulting from the multi-diffracted beam in the reference channel is

$$F_R(k) = \sum_{n=-\infty}^{\infty} e^{i2\pi(f_L+f_R+nF)t}\int_{-\frac{d_R}{2}}^{\frac{d_R}{2}} e^{-c_R x^2 - i2\pi(\frac{f_R+nF}{v}+k)x}dx \tag{4}$$

One of the reference beams is directed toward the signal channel light distribution (3) in the k-plane. However, because the other reference beams also overlap the signal beam to some extent, spurious output signals occur. If a high bandwidth efficiency is required, then the beams must overlap more, which implies a higher level of spurious signals.

The total light intensity in the k-plane is

$$|F_S + F_R|^2 = |F_S|^2 + |F_R|^2 + 2ReF_S F_R^* \tag{5}$$

By suitably filtering the photodetector output, the only important contribution to the output will be the cross product $G(k) = \mathrm{Re}\, F_S F_R^*$. The photocurrent is proportional to the integral of the intensity over the photosensitive area:

$$I = \int_{k_0-\frac{K}{2}}^{k_0-\frac{K}{2}} G(k)dk \tag{6}$$

where k_o is the location of the photocell in the k-plane and K is the width of the photocell. Now let f_o be the nominal channel carrier frequency, and let $f = f_S - f_R$ represent the input frequency relative to this nominal frequency. Assume that the k-plane location k_o corresponds to the frequency f_o, so that $k_o = -f_o/v$. Then the photocell output, translated in frequency to baseband, reduces to

$$I = \sum_{n=-\infty}^{\infty} H_R(f, nF)\cos 2\pi(f - nF)t \tag{7}$$

where

$$H_R(f,nf') = \int_0^{D_S/\tau} e^{-j2\pi f'x} \int_0^{D_H/\tau} e^{-j2\pi f'y} \left[\cos\frac{2\pi}{\nu}(fx + nf'y) \frac{\sin \pi k(x-y)}{x-y} + \right. \quad (8)$$

$$\left. \cos\frac{2\pi}{\nu}(fx - nf'y) \frac{\sin \pi k(x+y)}{x+y} \right| dx\,dy \quad (9)$$

The function $H_R(f,0)$ is the transfer function which will be denoted $H_R(f)$, and which can be calculated by numerical integration after the system parameters have been selected. The terms for which n=0 give the amplitudes of the spurious sinusoids.

Figure 4 is the computed transfer function for a particular set of MCD parameters. The parameters were selected to give the minimum bit error probability in the presence of ACI and ISI when the earth station transmissions are filtered with fifth-order Butterworth filters having time-bandwidth products of 0.5. A bandwidth efficiency of 1.6 bps/Hz has been assumed. We now describe the method used to compute the ACI and ISI, and then the bit error probability itself.

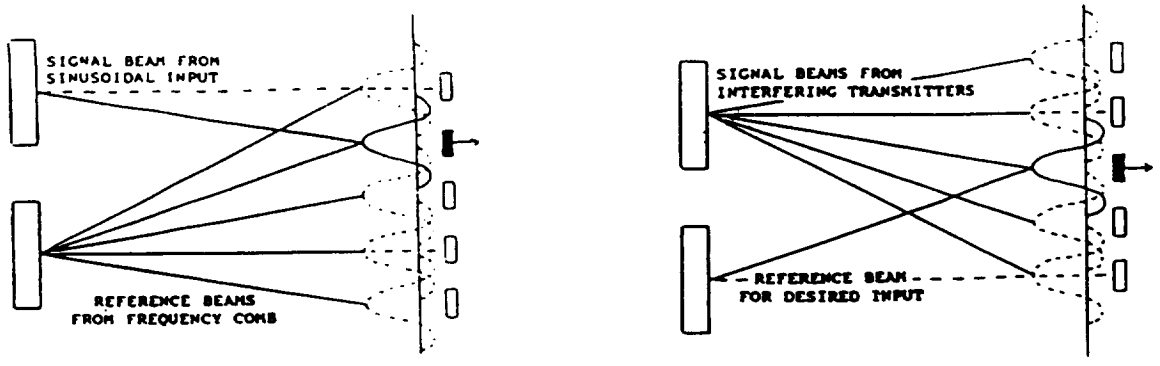

(a) Spurious Signal Distribution from Reference Comb

(b) ACI Distribution from Interfering Transmitters

Fig. 3 Interference Effects

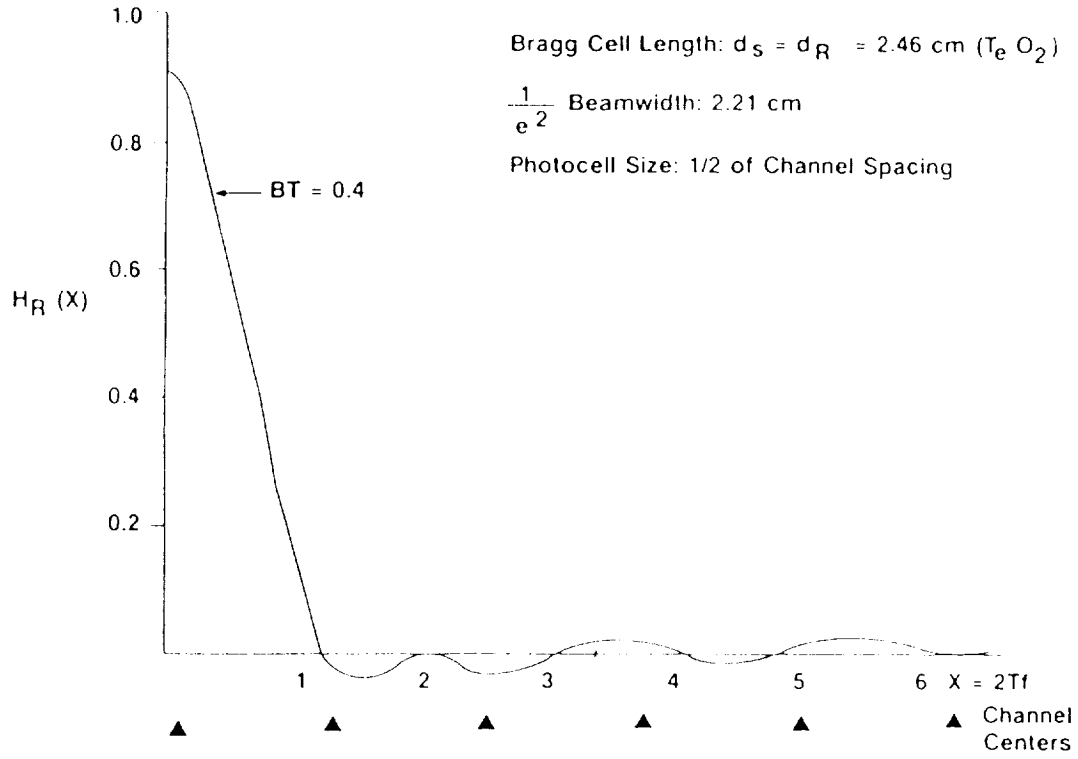

Fig. 4 MCD Transfer Function

ADJACENT CHANNEL INTERFERENCE

Design of any bandwidth-efficient FDMA system involves a fundamental trade-off. If the system bandwidth is narrow, we achieve good ACI performance at the cost of high ISI. Widening the bandwidth reduces the ISI but increases the ACI. The design procedure is generally to select filter types and bandwidths that give the best bit error performance in the presence of both ACI and ISI. We first consider the ACI.

Each ground transmitter is assumed to include bandpass filtering to reduce the amount of ACI entering the satellite receiver. As a first approximation for performance analysis, the demultiplexer can be treated conventionally as a bank of bandpass filters, each followed by a demodulator. The model is later generalized to take into account the spurious signals that are characteristic of the demultiplexer implementation.

It is straightforward to compute the ACI under the assumption that the interference can be treated as noise that adds to the thermal noise at the receiver input. This assumption is valid when there is a large number of interfering users because according to the central limit theorem, this implies that the interference has nearly Gaussian statistics. We also assume for simplicity that all transmissions arrive at the satellite with equal power.

The unfiltered spectral density of the n-th QPSK-modulated interfering signal is

$$S(f - nF) = \left[\frac{\sin 2\pi T(f - nF)}{2\pi T(f - nF)}\right]^2 \qquad (10)$$

All ground transmitters have identical filters, and the n-th filter transfer function is denoted by $H_T(f-nF)$. Thus the filtered transmission from the n-th interferer has a spectral density given by $S(f-nF)|H_T(f-nF)|^2$ Suppose the transfer function of the on-board demultiplexer is $H_R(f)$, which was evaluated in the previous section. Then the spectral density of the interference into the demodulator is

$$\sum_{n\neq 0} S(f - nF)|H_T(f - nF)H_R(f)|^2 \qquad (11)$$

Assume that the symbol detector is a filter matched to the undistorted symbol (i.e. an integrate-and-dump detector). Its transfer function is $H_{MF}(f)=\sin(2\pi Tf)/\ 2\pi Tf$. Then the total ACI power out of the matched filter relative to the undistorted signal power is

$$I = \sum_{n\neq 0} \int_{-\infty}^{\infty} S(f - nF)|H_T(f - nF)H_R(f)H_{MF}(f)|^2 df \qquad (12)$$

This is added to the thermal noise to estimate the error probability.

INTERSYMBOL INTERFERENCE

Unlike the ACI, the ISI cannot be accurately approximated as additive Gaussian noise. Instead, we determine explicitly the effect of the transmitter and receiver filtering on the amplitude of the signal out of the integrate-and-dump detector.

Expressing any one of the unfiltered QPSK signals before transmission as $s(t) = m(t)\cos(2\ f\ t +\ \ )$, the complex modulation is

$$m(t) = \frac{1}{\sqrt{2}} \sum_{n=-\infty}^{\infty} \left[a_n \,\mathrm{rect}\left(\frac{t - 2nT}{2T}\right) + ib_n \,\mathrm{rect}\left(\frac{t - (2n-1)T}{2T}\right)\right] \qquad (13)$$

where a and b are binary data on the I- and Q- channels respectively, which are assumed to be offset 1/2-symbol. The modulation spectrum of the filtered and demultiplexed signal at the input to its demodulator is $\hat{M}(f) = M(f)H_T(f)H_R(f)$, where M(f) is the spectrum of the undistorted QPSK modulation. The Fourier transform of this is the distorted modulation, which we will call $\hat{m}(t)$, and the output of the I-channel integrate-and-dump detector in the demodulator is

$$\frac{1}{2T}\int_{-T+\tau}^{T+\tau} \hat{m}(t)dt = T\sum_{n=0}^{\infty} a_{-n} \int_{-\infty}^{\infty} H_T(f)H_R(f)\left(\frac{\sin 2\pi Tf}{2\pi Tf}\right)^2 e^{i2\pi(2nT+\tau)f} df \qquad (14)$$

where τ is the sampling time relative to the symbol transition. The Q-channel output is similar. Because the filters introduce group delay, the sampling time is generally nonzero. We can split the composite transfer function $H_T(f)H_R(f)$ into its real and imaginary parts denoted by $\alpha(f)$ and $\beta(f)$ respectively. Because α is an even function of f and β is odd, the signal amplitude out of the I-channel of the detector becomes

$$S = 2\sum_{n=0}^{\infty} a_{-n} \int_0^{\infty} \left(\frac{\sin \pi x}{\pi x}\right)^2 \left[\alpha(x)\cos 2\pi\left(n + \frac{\tau}{2T}\right)x - \beta(x)\sin 2\pi\left(n + \frac{\tau}{2T}\right)x\right] dx \qquad (15)$$

after changing the integration variable. This shows that the detector output includes contributions from not only the desired (n=0) symbol, but from all symbols, which is what is meant by intersymbol interference. The bit error probability can be estimated from either the I-channel or Q-channel output.

By differentiation, we find that the value of for which the average value of S is a maximum is the solution of

$$\int_0^{\infty} \left(\frac{\sin \pi x}{\pi x}\right)^2 \left[\alpha(x)\sin\frac{\pi\tau x}{T} + \beta(x)\cos\frac{\pi\tau x}{T}\right] dx = 0 \qquad (16)$$

Once the optimum τ is found we can compute the contribution to S from the n=0 symbol and from all important interfering symbols. It has been found that the n = 1,2, 3, and -1 interfering symbols are the important ones in our application.

The bit error probability is then computed by averaging the error probability, conditioned on a particular sequence of these interfering symbols, over all 16 possible sequences of these symbols. The noise in this computation consists of the ACI, which was calculated in the previous section, plus the thermal noise at the input to the satellite receiver. If N_o is the thermal noise density at the input, the thermal noise power at the output of the integrate-and-dump detector is

$$N_0 \int_{-\infty}^{\infty} |H_R(f)H_{MF}(f)|^2 df \qquad (17)$$

which is added to the ACI in the error probability computation.

RESULTS

Having derived the demultiplexer transfer function, and having calculated the ACI and ISI, it is ,straightforward to write down an expression for the total power out of the device:

$$P = \sum_n \sum_m \int_{-\infty}^{\infty} S(f - nF)|H_T(f - nF)H_R(f, mF)H_{MF}(f)|^2 df \qquad (18)$$

The first sum is over the number of interfering earth stations, while the second is over the number of spurious signals produced by the reference beams. The m=n=0 term is the desired output; the m=0, n≠0 terms are the ACI; the m≠0, n=0 terms are the spurious outputs when there is only one uplink signal; and the m≠0, n≠0 terms are additional spurious outputs arising from interaction of the interfering channels with the n≠0 reference beams. Of this latter category, the m=n terms dominate, so they are included in the performance calculation. The m≠n interaction terms are illustrated in Fig. 2.

Figure 6 shows the bit error probability when the MCD transfer function is that shown in Fig. 4. Fifth-order Butterworth filters are used in the earth station transmitters, and integrate-and-dump symbol detection is assumed. The effects of ACI, spurious signals, and ISI are all included in the calculation. Also shown for comparison is a case where the optical MCD is replaced by a bank of bandpass fifth-order Butterworth filters whose bandwidths are optimized to give the smallest bit error probability in the presence of the same interference. Figure 6 shows that the performance of an optical MCD compares favorably with that of an MCD implemented electronically.

Figure 7 shows the sensitivity of system performance to timing errors in the symbol detection circuitry. This is evaluated by varying the sampling time about its optimum value when computing the error probability. It is evident that when the timing error is less than approximately ten percent of the symbol duration, its contribution to bit error degradation is insignificant compared to the ACI, spurious signals, and ISI.

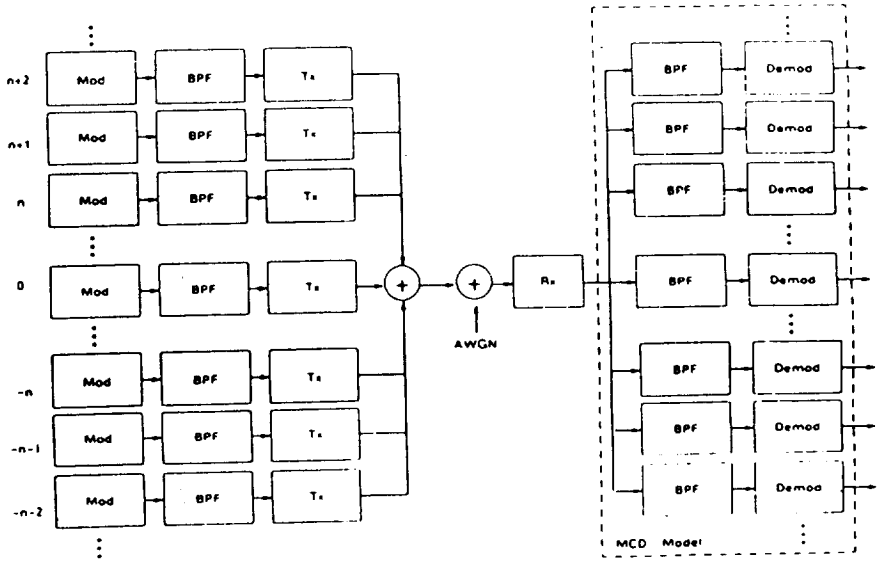

Fig. 5 Analytical Model for Performance Evaluation

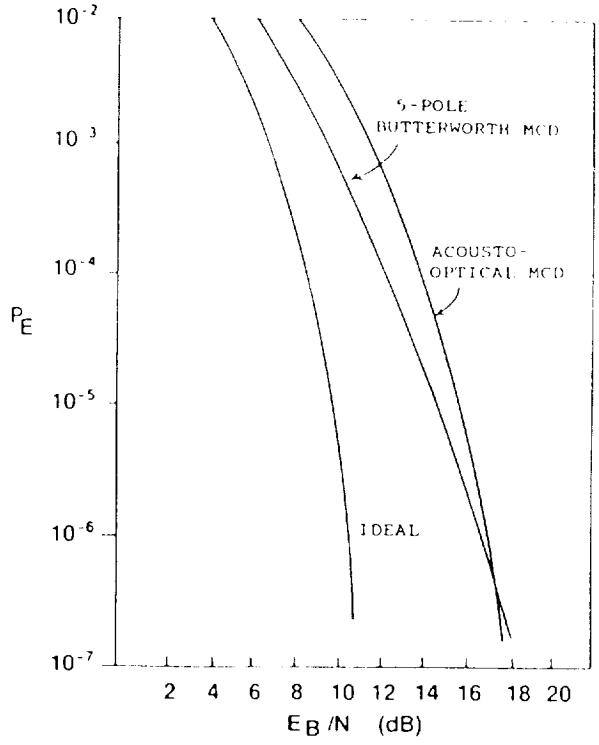

Fig. 6 Bit Error Probability

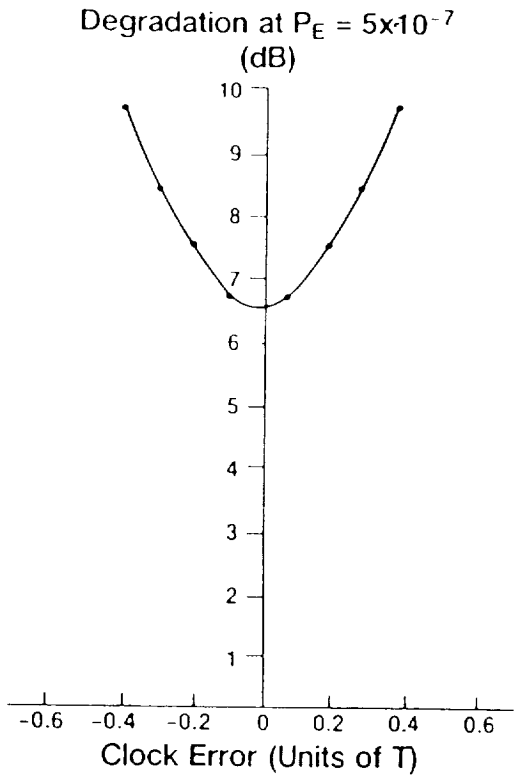

Fig. 7 Sensitivity to Symbol Synchronization Error

DISCUSSION AND CONCLUSION

The goal of this effort was to evaluate the performance of an optically implemented on-board demultiplexer that can service inexpensive, low-power earth stations. For such earth stations, no attempt has been made to improve bandwidth efficiency by using advanced modulation and coding schemes. In addition, we have assumed that no effort has been made to minimize ISI by careful design of the earth station transmitter filters. We have shown that an optically implemented MCD, which promises size and weight advantages over other implementations of on-board processors, can perform as well as other implementations so far as bit error probability is concerned.

However, to achieve comparable performance with the optical MCD, whose transfer function must be carefully controlled, it was found necessary to reduce the ground transmitter filter bandwidths. As seen in Fig. 6, this worsens performance at low signal-to-noise ratios because of the increased ISI that results. The optical MCD transfer function (Fig. 4) has amplitude and phase characteristics different from most classical filter responses. Also, spurious responses from the reference beams exist. Therefore, the ACI/ISI trade-off for an optical implementation differs significantly from that for an electronic one.

REFERENCES

[1] Ananasso, F. and Saggese, E., "A survey on the Technology of multi-carrier Demodulators for FDMA/TDMA User-oriented Satellite Systems", IEEE International Conference on Communications, Chicago, 1985, pp. 6.6.1 - 6.1.7.

[2] Ananasso, F. and Del Re, E., "Clock and Carrier Synchronization in FDMA/TDMA User-oriented Satellite Systems", IEEE International Conference on Communications, Seattle, 1987, pp. 41.7.1 - 41.7.5.

[3] Kappes, J. and Sayegh, S., "Programmable Demultiplexer/Demodulator Processor", IEEE Military Communication Conference, Monterey, 1990, pp. 7.3.1 - 7.3.5.

[4] Goutzoulis, A. and Abramovitz, I. "Digital Electronics Meets Its Match", IEEE Spectrum, Aug. 1988, pp. 21-25.

[5] Ananasso, F. and Bennion, I., "Optical Technologies for Signal Processing in Satellite Repeaters", IEEE Communications Magazine, Feb. 1990, pp. 55-64.